Biosensors and Bioelectronics 126 (2019) 785–791

Contents lists available at ScienceDirect

Biosensors and Bioelectronics

journal homepage: www.elsevier.com/locate/bios

# Sandwich-type electrochemical immunosensor for sensitive detection of CEA based on the enhanced effects of Ag NPs@CS spaced Hemin/rGO

Chunyan Zhang, Shuan Zhang, Yilei Jia, Yueyun Li*, Ping Wang, Qing Liu, Zhen Xu, Xinjin Li, Yunhui Dong

*School of Chemical Engineering, Shandong University of Technology, Zibo 255049, PR China*

ARTICLE INFO

*Keywords:*
Sandwich-type electrochemical immunosensor
Hemin/rGO
Spacer
Porous structure
Carcinoembryonic antigen

ABSTRACT

An ultrasensitive sandwich-type electrochemical immunosensor was designed by using gold nanoparticles (Au NPs) as the substrate material and microporous carbon spheres (CS) loading silver nanoparticles (Ag NPs) spaced Hemin/reduced graphene oxide (Hemin/rGO) porous composite materials (Ag NPs@CS-Hemin/rGO) as the detection antibodies ($Ab_2$) label for detecting carcinoembryonic antigen (CEA). The Au NPs with good electrical conductivity and biocompatibility could accelerate the electron transfer on the electrode interface and enhance the load capacity of capture antibodies ($Ab_1$). Hemin is peroxidase-like substance which has excellent catalytic ability for $H_2O_2$ reduction but easy to molecular aggregation and oxidative self-destruction. Reduced graphene oxide (rGO) is a good supporting material for Hemin to mitigate this disadvantage. CS loading Ag NPs (Ag NPs@CS) as the spacer inserts into Hemin/rGO sheet can overcome the irreversible stacking of rGO, and form complex porous structure which exposes more active sites of Hemin. Moreover, Ag NPs loaded on CS also has catalytic ability for $H_2O_2$ reduction. Thus the Ag NPs@CS-Hemin/rGO used as the $Ab_2$ label has a large working surface area and high utilization rate, which heightens the catalytic ability for $H_2O_2$ reduction to amplify the current signal effectually. The current signal and the logarithm of CEA concentration presented a wide linear response range of 20 fg/mL to 200 ng/mL, and the detection limit of CEA was 6.7 fg/mL. Furthermore, the designed immunosensor exhibited a good reproducibility, selectivity and stability, which confirms a broad development prospect when applying it in early clinical detection.

## 1. Introduction

Malignant tumor has been high morbidity and mortality disease which endangers human health seriously. According to the latest date (February 2018) of world health organization (WHO), nearly one in six deaths was caused by cancer and the number of new cases will continue increase in the next two decades. Carcinoembryonic antigen (CEA) is a reliable broad spectrum tumor marker, which concentration in human serum is below 5 ng/mL (Majuri et al., 1994), but it rises when the tumors existence in many organs (e.g. large intestine, mammary gland and lung) (Gu et al., 2018). The CEA is also recognized as an effective prognostic indicator for monitoring the stage of cancer in clinical assays (Alsabti, 1979). So, accurate and quantitative detection of CEA by highly sensitive and simple method has great application value for early clinical diagnosis of tumor (Wu et al., 2015).

Until now, various methods of CEA detecting have been proposed such as enzyme-linked immunosorbent assay (Wischhusen and Padilla, 2017), electrochemiluminescence immunoassay (N.-L. Li et al., 2017), radioimmunoassay (Chou et al., 2004) and electrochemical immunosensor (Rizwan et al., 2018). Electrochemical immunosensor which based on the specific combination of antigen and corresponding antibody has gained wide attention due to its significant advantages involving high sensitivity, low detection limit, fast response, easy to handle and low manufacturing cost (Felix and Angnes, 2017; Amani et al., 2018). And sandwich-type electrochemical immunosensor is outstanding. The signal amplification strategy, which involves substrate material and the nanomaterial conjugated with detection antibodies ($Ab_2$), plays an important role in the sandwich-type electrochemical immunosensor for sensitive detection.

In this work, an ultrasensitive sandwich-type electrochemical immunosensor for CEA detection was designed by applying the gold nanoparticles (Au NPs) as the substrate material and microporous carbon spheres (CS) loading silver nanoparticles (Ag NPs) spaced Hemin/reduced graphene oxide (Hemin/rGO) porous composite materials (Ag NPs@CS-Hemin/rGO) as $Ab_2$ label. Recently, Au NPs has been used as substrate material in immunosensor extensively due to its good

* Corresponding author.
*E-mail address:* liyueyun@sdut.edu.cn (Y. Li).

https://doi.org/10.1016/j.bios.2018.11.039
Received 9 August 2018; Received in revised form 23 November 2018; Accepted 26 November 2018
Available online 07 December 2018
0956-5663/ 

electrical conductivity and excellent biocompatibility (Mani et al., 2009; Zapp et al., 2014). Au NPs could accelerate the electron transfer rate and provide a good microenvironment for incubation of capture antibody ($Ab_1$), thereby the stability of the sensor interface construction was improved (M. Li et al., 2018).

The designed immunosensor for quantitative determination of CEA was also based on the $Ab_2$ label as the excellent signal amplifier. Hemin is peroxidase-like substance in which the porphyrin ring composed of four pyrrole rings, and the nitrogen atom on the pyrrole rings coordinated with a ferrous ion ligand (Li et al., 2018a). The electron conjugated system with π bond and the changes in the valence state of iron ions made Hemin a good catalytic ability for $H_2O_2$ reduction with its specific redox properties (Liang et al., 2011). Whereas, it is still a significant challenge for applying the Hemin as the oxidation catalyst because of its molecular aggregation could form catalytic inactive dimers in aqueous solution and oxidative self-destruction in the oxidizing media, which reduce its catalytic activity (Xue et al., 2012). Therefore, a supporting material with large surface area is highly demanded to attain the stability and activity of the Hemin. Reduced graphene oxide (rGO) has been widely applied to the construction of working electrode sensing interfaces because of good conductivity, well biocompatibility, large specific surface area and easy to functionalization and compounding (Singh et al., 2016; Li et al., 2014). The porphyrin ring of Hemin and the six-membered ring structure of rGO could be combined by π bonded (Guo et al., 2011), so the rGO could be used as the supporting material for Hemin. The Hemin/rGO synthesized the large surface area of rGO and the biomimetic catalytic activity of Hemin, which greatly improved the catalytic performance of $H_2O_2$.

However, rGO tends to be irreversibly stacked so that the catalytic activity sites of Hemin/rGO would decrease badly. CS with a large diameter could be used as the spacer to support the sheet layers of Hemin/rGO and provide large surface area. Ag NPs has a good electrical conductivity and well biological compatibility (Ma et al., 2016) which can load on CS to improve the catalytic ability for reduction of $H_2O_2$ (Li et al., 2018b). CS loading Ag NPs (Ag NPs@CS) made the Ag NPs@CS exhibiting both the spacing function of CS and the catalytic ability of Ag NPs. Ag NPs@CS as the spacer inserted into the Hemin/rGO not only can form the gap between Hemin/rGO layers to reduce the stacked phenomenon, but also make the Ag NPs@CS-Hemin/rGO to form complex porous structure and large specific surface area. The porous structure exposed more active reaction sites produced by Hemin and Ag NPs, which increased the utilization of Ag NPs@CS-Hemin/rGO. And the large specific surface area provided more reactivity sites to improve the catalytic activity for reduction reaction of $H_2O_2$. Consequently, with the fine cooperation of Ag NPs@CS and Hemin/rGO, the Ag NPs@CS-Hemin/rGO as the $Ab_2$ label applied to the designed immunosensor has achieved sensitive detection of CEA with superior reproducibility, stability and selectivity. The designed immunosensor has a good correlation with commercial ELISA when used in real human serum samples detection, which indicates a good expectation in clinical application.

## 2. Experimental

### 2.1. Reagents and apparatus

CEA and CEA antibody were purchased from Linc-Science Co., Ltd. (Shanghai, China). Human CEA ELISA Kit was purchased from Hushang Biochemical Reagents Co., Ltd. (Shanghai, China). Bovine serum albumin (BSA, 96–99%) was purchased from Sigma reagent Co., Ltd. (St. Louis, MO, USA). Chloroauric acid ($HAuCl_4{\cdot}4H_2O$) were obtained from Sigma-Aldrich Co., Ltd. (Beijing, China). Resorcinol ($C_6H_6O_2$) and formaldehyde ($CH_2O$) were purchased from Aladdin Chemistry Co., Ltd. (Shanghai, China). Silver nitrate ($AgNO_3$) and sodium citrate ($Na_3C_6H_5O_7{\cdot}2H_2O$) were obtained from Macklin Biochemical Co., Ltd. (Shanghai, China). Sodium borohydride ($NaBH_4$) was obtained from Energy chemistry Co., Ltd. (Shanghai, China). Hemin and 2-aminopyridine ($C_5H_6N_2$) were purchased from Macklin Biochemical Co., Ltd. (Shanghai, China). Potassium ferricyanide ($K_3[Fe(CN)_6]$) and potassium ferrocyanide ($K_4[Fe(CN)_6]$) were purchased from Sinopharm Chemical Reagent Co., Ltd. (Beijing, China). Phosphate buffered saline (PBS, 1/15 mol/L) was prepared by compounding the solution of disodium hydrogen phosphate ($Na_2HPO_4$) and potassium phosphate monobasic ($KH_2PO_4$). The level of other chemicals and solvents was of analytical grade, and used without further purification. Ultrapure water (18.25 MΩ cm, 24 °C) was made by Ulupure UPT-II-15T laboratory ultra-pure water system (Sichuan Ulupure super pure technology co. LTD) and used in all the experimental processes.

All electrochemical measurements were performed on CHI760E electrochemical workstation (Shanghai Chenhua Instruments Co., China) using a conventional three-electrode system which consisted of a glassy carbon electrode (GCE, 4 mm in diameter) as the working electrode, a saturated calomel electrode (SCE) as the reference electrode and a platinum wire electrode as the counter electrode. Transmission electron microscope (TEM) images were obtained from Tecnai G2 F20 S-TWIN transmission electron microscope (Field Electron and Ion Co., United States). Scanning electron microscope (SEM) images were obtained using Quanta FEG250 field emission environmental SEM with energy-dispersive spectrometer (EDS) analysis (Field Electron and Ion Co., United States). Nitrogen ($N_2$) adsorption-desorption data was obtained by using an ASAP 2020 apparatus (Micromeritics Instrument Co., United States).

### 2.2. Preparation of Au NPs

The preparation of Au NPs was according to a typical method (Frens, 1973). First, 1.0 mL of 1.0 wt% $HAuCl_4{\cdot}4H_2O$ was added into 99.0 mL of ultrapure water, and refluxed at 100 °C to boiling. Then 2.5 mL of 1.0 wt% sodium citrate was added into the solution, kept stirring for 15 min. A wine red solution containing Au NPs was obtained.

### 2.3. Preparation of Ag NPs@CS

The preparation of Ag NPs colloid was as follows. First, 1.0 mL of $AgNO_3$ (50.0 mmol/L) solution and 1.0 mL of 5.0 wt% sodium citrate solution was added to 48.0 mL ultrapure water under magnetic stirring. Then, cautiously add, dropwise, $NaBH_4$ solution (0.01 wt%) to above solution, and keep magnetic stirring for 10 min.

The preparation of CS was according to our previous research (Zhang et al., 2018) with a little modifying. Briefly, 20.0 mg of CS was added to 30.0 mL of Ag NPs colloid, and then oscillated the mixture at room temperature for 8 h. After centrifugation, the obtained Ag NPs@CS was re-dispersed in 2.0 mL of ultrapure water and stored at 4 °C for further use.

### 2.4. Preparation of graphene oxide

Graphene oxide (GO) was prepared by an improved Hummer's method (Hummers Jr and Offeman, 1958). First, 2.0 g graphite flakes were added slowly to 100.0 mL of concentrated sulfuric acid under 0 °C ice bath with magnetic stirring. Then, 1.0 g $KNO_3$ and 12.0 g $KMnO_4$ were added slowly to the mixture, and continue 0 °C ice bath with magnetic stirring for 90 min. Next, the mixture was transferred to oil bath, reacted 120 min at 50 °C with magnetic stirring, then heat up to 55 °C, and kept stirring for 180 min. After that, 300.0 mL of ultrapure water was added to the mixture dropwise. Then, 18.0 mL of 30.0 wt% $H_2O_2$ was added, kept magnetic stirring for 5 min. After 12 h standing at room temperature, golden yellow precipitate of the mixture was purified by 7 days dialysis. Finally, 1.0 g precipitate was added to 300.0 mL ultrapure water, after sonicating continuously for 30 min and centrifuging at 4500 rpm for 5 min, the supernate was dried by freeze-drying method.

### 2.5. Preparation of $Ab_2$ label

Ag NPs@CS-Hemin/rGO was prepared by a one-step hydrothermal process. First, 5.0 mg of Hemin and 5.0 g of 2-aminopyridine were added to 50.0 mL of GO (1.0 mg/mL), a dark brown homogeneous solution was obtained after sonicating continuously for 45 min. Then, 10.0 mL of Ag NPs@CS (10.0 mg/mL) was added to the solution under magnetic stirring, and kept magnetic stirring for 10 min. Next, the mixture was transferred to a Teflon lined autoclave for solvothermal reaction at 130 °C for 3 h. The black precipitate was obtained by consecutive washing/centrifugation cycles five times with ultrapure water and ethanol. The obtained precipitate (Ag NPs@CS-Hemin/rGO) was dried by freeze-drying method.

After that, 1.0 mL of Ag NPs@CS-Hemin/rGO (3.0 mg/mL) was mixed with 1.0 mL of $Ab_2$ solution (20.0 μg/mL) and oscillated at 4 °C for 12 h. Then, the mixture was centrifuged and rinsed with PBS (pH = 7.0) to remove the unbound $Ab_2$. The obtained Ag NPs@CS-Hemin/rGO-$Ab_2$ ($Ab_2$ label) was re-dispersed in 2.0 mL of PBS (pH = 7.0) and stored at 4 °C for further usage.

### 2.6. Fabrication for working electrode of the immunosensor

Fig. 1 illustrates the fabrication process for working electrode of the immunosensor. Before modifying the surface of electrodes, the GCE was polished by alumina polishing powders with particle size of 1.0, 0.3, and 0.05 μm in sequence, followed by sonication in ethanol and rinsed by ultrapure water. Then, the surface of GCE was covered with 7.0 μL of Au NPs colloid and dry at room temperature. Next, the integrate Au NPs/GCE was covered with 6.0 μL $Ab_1$ (10.0 μg/mL) and dried at 4 °C. After rinsing with PBS (pH = 7.0), 3.0 μL of BSA solution (1.0 wt%) was dropped onto the surface of modified electrode to block the remaining active sites, eliminate non-specific adsorption of proteins. After 1 h incubation, the surface of modified electrode was rinsed with PBS (pH = 7.0) and covered by 6.0 μL of CEA solution with a series of concentrations at 4 °C for 1 h to ensure the specific binding between CEA and $Ab_1$. Each concentration of CEA was modified on a correspond electrode respectively. Finally, 6.0 μL of $Ab_2$ label (1.5 mg/mL) was added to the surface of modified electrode, and stored at 4 °C for 45 min. The prepared working electrodes were rinsed with PBS

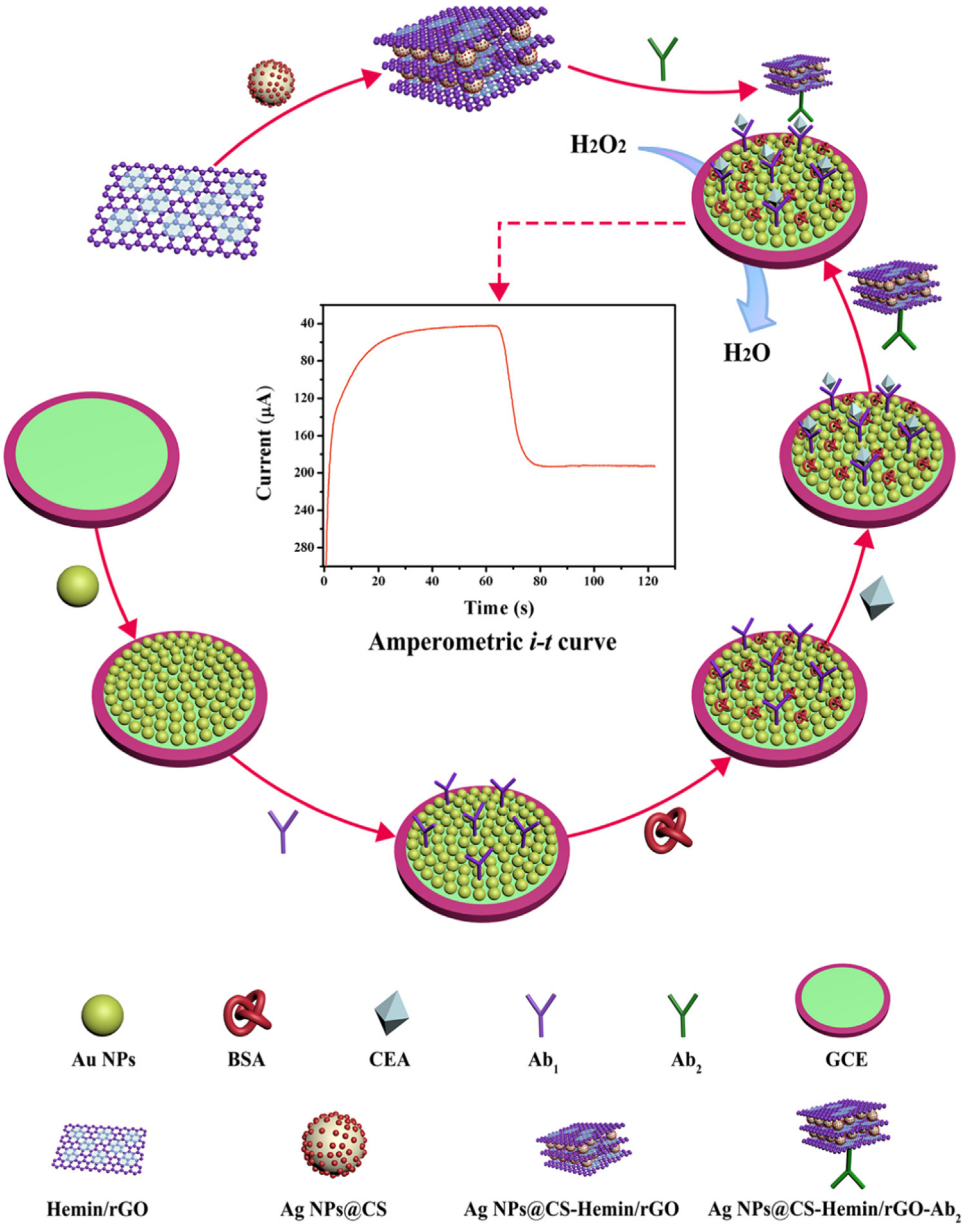


**Fig. 1.** The procedure of sandwich-type immunosensor working electrode.

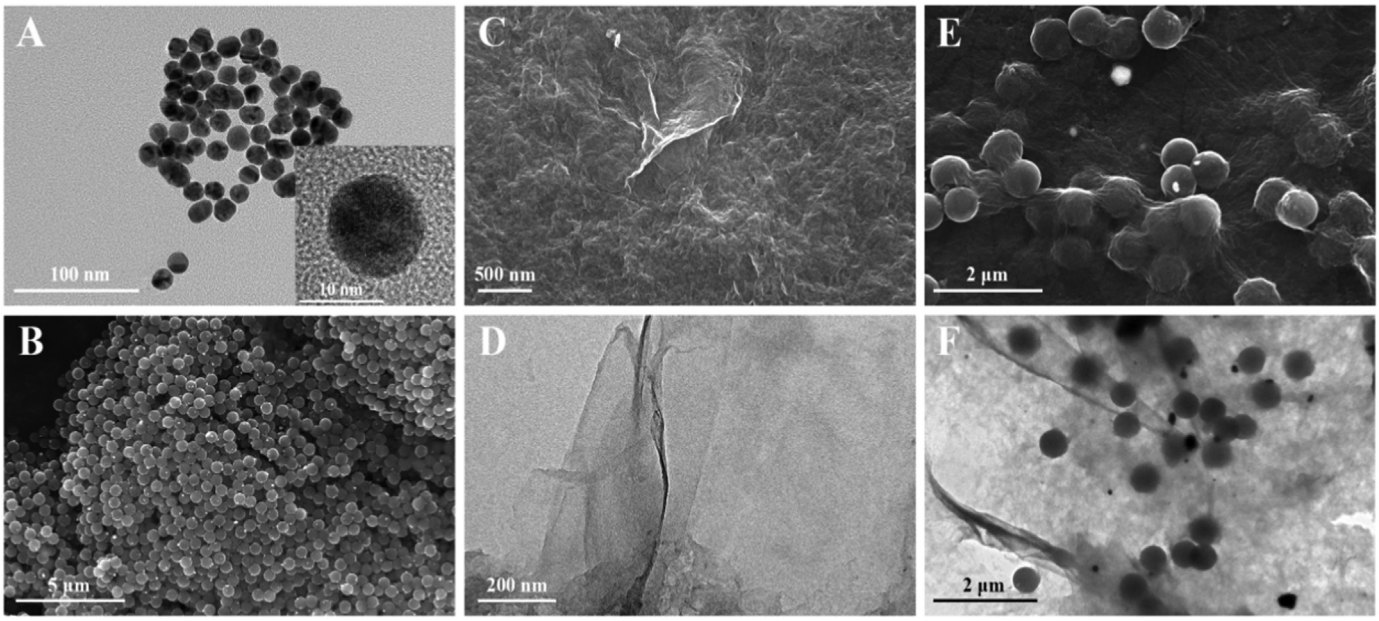


**Fig. 2.** (A) TEM image of Au NPs (inset: high-resolution TEM image of Au NPs); (B) SEM image of Ag NPs@CS; (C) SEM image of Hemin/rGO; (D) TEM image of Hemin/rGO; (E) SEM image of Ag NPs@CS-Hemin/rGO; (F) TEM image of Ag NPs@CS-Hemin/rGO.

(pH = 7.0) to remove the unbound $Ab_2$ label and stored at 4 °C for further measurement.

### 2.7. Detection of CEA

Amperometric *i-t* curve was used to measure the electrochemical characteristics of the prepared working electrodes, and −0.4 V was selected as detection potential for amperometric measurements. Amperometric *i-t* curve was performed in 10.0 mL of PBS (pH = 7.0), inject 10.0 μL of $H_2O_2$ (5.0 mol/L) into the PBS under mild stirring when the background current was stabilized and record the change of current signal.

## 3. Results and discussion

### 3.1. Characterization of Au NPs, Ag NPs@CS, Hemin/rGO and Ag NPs@CS-Hemin/rGO

Fig. 2A presents the TEM image of Au NPs which formed uniform globular morphology with the average size of 13 nm. Fig. 2B shows the SEM image of Ag NPs@CS. The prepared CS formed uniform spherical morphology with Ag NPs loaded, and the average diameter was about 500 nm. Fig. S1 shows the EDS image of Ag NPs@CS which proved the elemental composition was Ag and C and the Ag NPs were loaded on the CS uniformly. Fig. 2C shows the SEM image of Hemin/rGO, which displayed rough surface but stacking of layers. Fig. 2D shows the TEM image of Hemin/rGO, a thin layer of Hemin/rGO was observed clearly. Besides, Fig. S2A, B and C show the C, N and Fe elemental mapping of Hemin/rGO respectively and Fig. S2D displays the comprehensive mapping of C, N and Fe elements, N and Fe elements are distributed uniformly which indicated Hemin was introduced into the rGO successfully and dispersed homogeneously. Fig. 2E and F give the SEM image and TEM image of Ag NPs@CS-Hemin/rGO respectively. As shown in Fig. 2E, Ag NPs@CS was wrapped in layers of Hemin/rGO. The TEM image of Ag NPs@CS-Hemin/rGO illustrates Ag NPs@CS inserted into different thin layers of Hemin/rGO further. The spaced structure was formed successfully with many folds, which manifesting the phenomenon of stacking was obviously reduced. Furthermore, Fig. S3A, B, C and D show the elemental mapping of C, N, Ag and Fe elements respectively and Fig. S3E describes the comprehensive mapping of Ag NPs@CS-Hemin/rGO. N, Fe and Ag elements are distributed uniformly which demonstrated Hemin and Ag NPs@CS were dispersed homogeneously and the Ag NPs@CS-Hemin/rGO was manufactured successfully. Fig. S4A and Fig. S4B display the $N_2$ adsorption-desorption isotherm of Hemin/rGO and Ag NPs@CS-Hemin/rGO. The average pore size and the BET surface area of Hemin/rGO were 5.34 nm and 174.92 $m^2$/g. The average pore size and the BET surface area of Ag NPs@CS-Hemin/rGO were 13.58 nm and 383.24 $m^2$/g. Ag NPs@CS as the spacer inserted into Hemin/rGO made the Ag NPs@CS-Hemin/rGO formed complex porous structure and large surface area, so the Ag NPs@CS-Hemin/rGO had a larger average pore size and the BET surface area than Hemin/rGO (details were shown in supplementary material). The $N_2$ adsorption-desorption isotherm attested that the Ag NPs@CS-Hemin/rGO with spaced structure was manufactured successfully. Briefly, Au NPs, Ag NPs@CS, Hemin/rGO and Ag NPs@CS-Hemin/rGO were successfully synthesized.

### 3.2. Electrochemical characterization

#### 3.2.1. Electrochemical characterization of Hemin/rGO and Ag NPs@CS-Hemin/rGO

Cyclic voltammetry (CV) and electrochemical impedance spectroscopy (EIS) test were carried out to investigate the electrochemical characterization of Hemin/rGO and Ag NPs@CS-Hemin/rGO. The CV test was performed by scanning the potential from −0.2–0.6 V with the direction of positive scan. As shown in Fig. 3A, the redox peak current of Hemin/rGO (curve b) was enhanced compared with the bare electrode (curve a). When the Ag NPs@CS-Hemin/rGO (curve c) was used to modify the electrode, it presented a most obvious redox peak current compared with Hemin/rGO and bare GCE. The CV comparison indicated the Ag NPs@CS-Hemin/rGO had a better electrocatalytic activity than Hemin/rGO, which could be attributed to the formation of spaced structure which exposed abundant catalytical active sites with inserting the Ag NPs@CS into Hemin/rGO.

Consistently, the electrochemical characterization of Hemin/rGO and Ag NPs@CS-Hemin/rGO was also evaluated by EIS. At high frequencies, a semicircle portion is observed and the diameter of semicircle corresponds to the surface electron-transfer resistance ($R_{et}$). From Fig. 3B, when modify the electrode with Hemin/rGO (curve b), the semicircle diameter was shortened compared with the bare GCE (curve

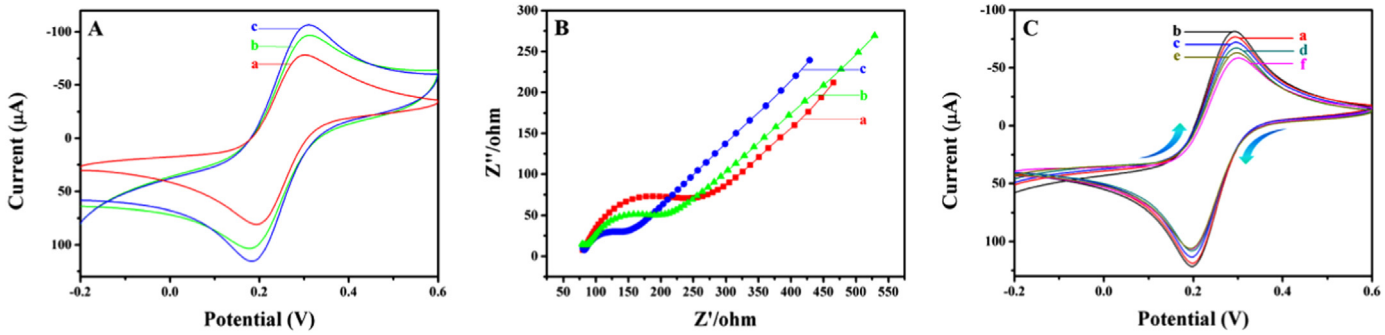


**Fig. 3.** (A) CV of GCE (a), Hemin/rGO modified GCE (b) and Ag NPs@CS-Hemin/rGO modified GCE (c) at the rate of 0.1 V/s; (B) EIS of GCE (a), Hemin/rGO modified GCE (b) and Ag NPs@CS-Hemin/rGO modified GCE (c) in the frequency range from 0.1 Hz to 100 kHz at a bias potential of 0.25 V; (C) CV of bare GCE (a), GCE/Au NPs (b), GCE/Au NPs/$Ab_1$ (c), GCE/Au NPs/$Ab_1$/BSA (d), GCE/Au NPs/$Ab_1$/BSA/CEA (e) and GCE/Au NPs/$Ab_1$/BSA/CEA/$Ab_2$ label (f) at the rate of 0.1 V/s. The test solution is 0.1 mol/L KCl contains 2.5 mmol/L $[Fe(CN)_6]^{3-/4-}$.

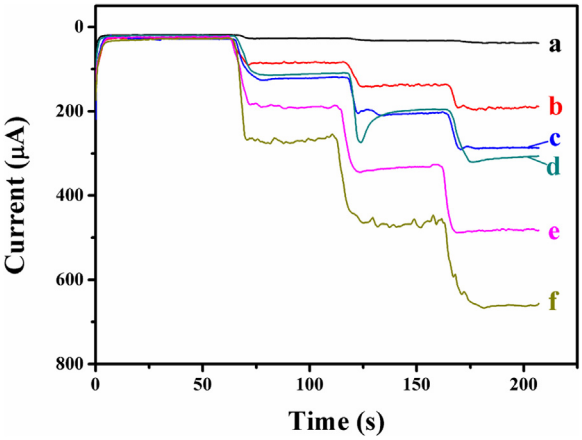


**Fig. 4.** The current responses of CS (a), Au NPs (b), Ag NPs (c), Ag NPs@CS (d), Hemin/rGO (e) and Ag NPs@CS-Hemin/rGO (f) which measured by amperometric *i-t* curve at the potential of −0.4 V in 10.0 mL of PBS (pH = 7.0) contains 5.0 mmol/L of $H_2O_2$.

a) at high frequencies, which indicated the $R_{et}$ decreased and the Hemin/rGO could accelerate the electron transfer. Furthermore, the Ag NPs@CS-Hemin/rGO (curve c) modified electrode had a shorter semicircle diameter than curve b which demonstrated the $R_{et}$ was further decreased. Ag NPs@CS as the spacer inserted into Hemin/rGO lent the Ag NPs@CS-Hemin/rGO obtained a faster charge transfer process and a better electrical conductivity than Hemin/rGO.

In order to further investigate the electrochemical characterization of Hemin/rGO and Ag NPs@CS-Hemin/rGO, the CV of the Hemin/rGO and Ag NPs@CS-Hemin/rGO modified electrodes was performed at different rates (0.01–0.1 V/s) in 0.1 mol/L KCl solution containing 5.0 mmol/L $K_3[Fe(CN)_6]$. As shown in Fig. S5, the reaction of $K_3[Fe(CN)_6]$ occurred on the electrode surface was a diffusion-controlled process (Chen et al., 2016). And the Randles-Sevcik equation (Zhang et al., 2016) was used to compare the effective working area of Ag NPs@CS-Hemin/rGO and Hemin/rGO modified electrodes: $A_{AgNPs@CS\text{-}Hemin/rGO}/A_{Hemin/rGO} = 1.264$ (calculated by cathodic peak current) and 1.338 (calculated by anodic peak current). The comparative result manifests that the effective working area of Ag NPs@CS-Hemin/rGO is larger than Hemin/rGO. Therefore, it can be concluded that the Ag NPs@CS inserted into the Hemin/rGO made the Ag NPs@CS-Hemin/rGO formed the spaced structure and greatly increased the effective working area (details were shown in supplementary material).

### 3.2.2. Electrochemical characterization of the immunosensor fabrication

CV was used to record each process of fabrication and to confirm the designed immunosensor was fabricated successfully. In this work, CV was performed by the potential of scanning from −0.2–0.6 V with the direction of positive scan as the arrow showed in Fig. 3C and the scan rate was chosen as 0.1 V/s. As shown in Fig. 3C, the process of CV was quasi-reversible process at the modified electrode. After modifying the surface of electrode with Au NPs (GCE/Au NPs, curve b), the redox peak current increased distinctly compare with bare GCE (curve a), because the Au NPs with excellent conductivity could accelerate electron transfer and reduce interface resistance. But when the $Ab_1$ (GCE/Au NPs/$Ab_1$, curve c), BSA (GCE/Au NPs/$Ab_1$/BSA, curve d), CEA (GCE/Au NPs/$Ab_1$/BSA/CEA, curve e) and $Ab_2$ label (GCE/Au NPs/$Ab_1$/BSA/CEA/$Ab_2$ label, curve f) were coated on the surface of electrode in sequence, the redox peak current decreased orderly because the bioactive substances greatly inhibited the efficiency of electron transfer. Therefore, the fabrication of immunosensor was completely successful.

### 3.3. Comparison of different signal amplification strategies

The electrocatalytic activity of various materials dominates the sensitivity of the fabricated electrochemical immunosensor. In order to investigate the signal amplification mechanism, different materials were modified on the surface of GCE and tested by amperometric *i-t* curve. As shown in Fig. 4, Au NPs (curve b) had a small but stable response current, indicates that Au NPs could uniformly adhere to the electrode surface and facilitate electron transfer between GCE and electrolyte, so it could be used as substrate material. A weak signal was detected when CS (curve a) was modified onto the electrode. Compared with the weak signal of CS, the response current of Ag NPs (curve d) increased obviously because Ag NPs has a good catalytic effect on reduction of $H_2O_2$ and electrical conductivity. When Ag NPs loaded on CS, the Ag NPs@CS (curve c) had the same property of Ag NPs, so the current response of Ag NPs had little difference with Ag NPs@CS. Compared with Ag NPs@CS (curve c) and Hemin/rGO (curve e), Ag NPs@CS-Hemin/rGO (curve f) generated the largest response current value. Owing to the formation of spacer and the synergistic effect of Ag NPs@CS and Hemin/rGO, the Ag NPs@CS-Hemin/rGO had an excellent catalytic ability towards the reduction of $H_2O_2$. Hence, the Ag NPs@CS-Hemin/rGO as the $Ab_2$ label improves the sensitivity of the designed immunosensor visibly.

### 3.4. Analytical performance of immunosensor

In order to obtain the best experimental conditions for detecting CEA, the pH of PBS, the volume of Au NPs colloid, the concentration of $Ab_2$ label and the incubation time of $Ab_2$ label were optimized, and the optimum value was 7.0, 7.0 μL, 1.5 mg/mL and 45 min respectively (details were shown in supplementary material). The designed electrochemical immunosensor was used to detect CEA by amperometric *i-t* curve under optimal conditions. Fig. 5A shows the current responses of

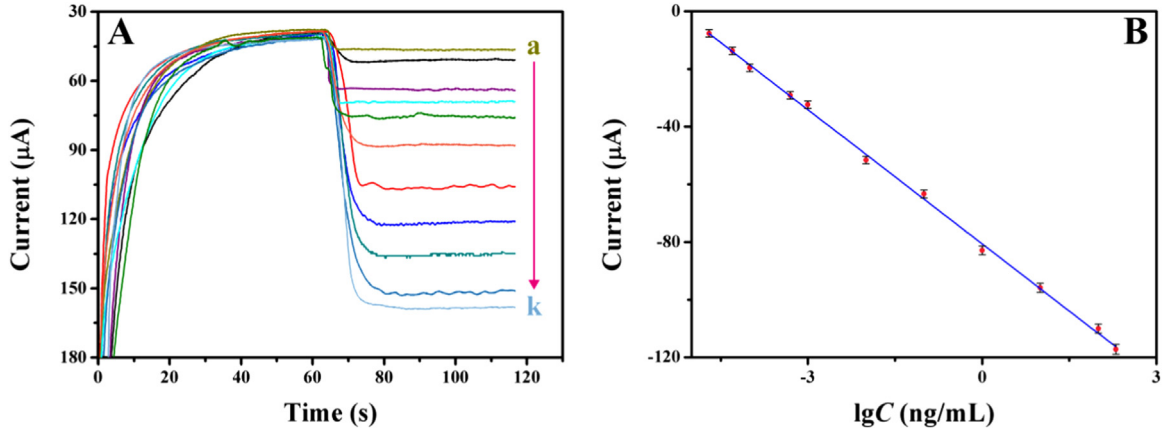


**Fig. 5.** (A) Amperometric *i-t* curve of the immunosensor to different concentrations of CEA at the potential of −0.4 V in 10.0 mL of PBS (pH = 7.0) contains 5.0 mmol/L of $H_2O_2$, from a to k: 20 fg/mL, 50 fg/mL, 100 fg/mL, 500 fg/mL, 1 pg/mL, 10 pg/mL, 100 pg/mL, 1 ng/mL, 10 ng/mL, 100 ng/mL, 200 ng/mL; (B) Calibration curve of the immunosensor to different concentrations of CEA, error bar = SD.

different concentrations of CEA. With the increase of CEA concentration, the current response was increased. As shown in Fig. 5B, the calibration plot showed a good relationship between the current difference ($\Delta I$) and the logarithm value of the CEA concentration within a range from 20 fg/mL to 200 ng/mL and the detection limit of CEA was 6.7 fg/mL at a signal-to-noise ratio of 3. The points in Fig. 5B were calculated by the equation: $\Delta I = I_0 - I_t$, which $I_0$ was the stabilized background current and $I_t$ was the current after inject the $H_2O_2$. The regression equation was $\Delta I = -15.513 \lg C - 80.633$ ($R^2 = 0.9986$), where $\Delta I$ (μA) is the response current of the immunosensor and $C$ (ng/mL) is the concentration of CEA. The result indicated the proposed immunosensor had a wide detection range and a low detection limit in the detection of CEA. In addition, the analytical performance of the designed immunosensor for CEA detection was compared with other immunosensors reported in the literatures, which was summarized in Table S1. As shown in Table S1, the designed immunosensor displayed a greater advance including higher sensitivity and wider linear range for the detection of CEA than previously reported. The advance of the designed immunosensor could be attributed to excellent performance of the designed signal amplification system. As the substrate, Au NPs could accelerate electron transfer and provide a suitable microenvironment for $Ab_1$ immobilized. The prepared Ag NPs@CS-Hemin/rGO has excellent catalytic ability for $H_2O_2$ which owing to the large working surface area and the synergistic effect of Hemin/rGO and Ag NPs@CS.

### 3.5. Reproducibility, stability and specificity of the immunosensor

The reproducibility is a significant indicator to evaluate the precision of the designed electrochemical immunosensor. A series of working electrodes were fabricated and divided into five groups (5 electrodes each group) to detect 1 pg/mL, 10 pg/mL, 100 pg/mL, 1 ng/mL, 10 ng/mL of CEA respectively. The immunosensors were detected by amperometric *i-t* curve under the optimal conditions. Fig. 6A shows the average peak current of these five groups of electrodes, and the relative standard deviation (RSD) was 3.32%, 3.21%, 2.82%, 3.09%, 2.56% respectively, which indicates that the designed electrochemical immunosensor has remarkable reproducibility.

The stability of the immunosensor was tested by detecting its current response periodically. Five working electrodes were fabricated to detect the CEA (1 ng/mL) under the optimal conditions, and were stored at 4 °C for further test. As shown in Fig. 6B, the current response of the immunosensor only changed 4.08% after 15 days and 9.97% after 24 days, and 84.94% of initial response remained even after storage for 30 days. The decrease of the peak current response may be caused by the aggregation or gradually inactivation of CEA and CEA antibody. The result of the detection indicates the designed immunosensor has acceptable stability.

To investigate the specificity of the designed immunosensor, interference study was performed by using alpha fetoprotein (AFP), hepatitis B surface antigen (HBs), prostate specific antigen (PSA) and human immunoglobulin (IgG). One ng/mL CEA with and without 10 ng/mL interfering substances solution was measured by the designed immunosensor. Fig. 6C gives the result of the study, compared with the current response caused by pure CEA, the variation in current caused by the interfering substances was less than 5%, indicates the proposed electrochemical immunosensor has fine selectivity and specificity.

### 3.6. Real sample analysis

To further investigate the feasibility and potential clinical application of the designed immunosensor, the detection performance of CEA in human serum sample was explored by standard addition methods in real sample (M. Li et al., 2017). The sample which analyzed by the designed immunosensor was spiked with 5 ng/mL, 10 ng/mL, 20 ng/mL of CEA solution and well recovery was obtained as shown in Table S2. The RSD of detecting results was from 1.01% to 2.43% and the recovery was from 99.48% to 100.56%, demonstrates the designed immunosensor has good sensitivity and accuracy. Table S3 shows the comparison between the results of the designed immunosensor and the commercialized available ELISA. As shown in Table S3, the relative deviation between the two methods was range from −1.81–2.21%. The result shows a good comparability between these two analytical methods, and provides further evidence that the designed immunosensor can be applied to the determination of CEA in clinical detection.

## 4. Conclusion

In summary, an ultrasensitive sandwich-type electrochemical immunosensor for CEA detection was constructed in this work. Au NPs was utilized as the substrate material to immobilize $Ab_1$ and accelerate the electron transfer on the electrode interface. The Ag NPs@CS-Hemin/rGO as the $Ab_2$ label could effectually amplify the current signal for its large working surface area and excellent catalytic ability toward the reduction of $H_2O_2$. Hence, the designed immunosensor exhibited a wide range linear response and a low detection limit. Credibly, the designed immunosensor also displayed a good reproducibility, high selectivity and acceptable stability. The sensitive and selective response of the immunosensor to CEA in real human serum samples was validated by the conventional ELISA, and this result provided a promising opportunity for real diagnosis. Hopefully, such an electrochemical

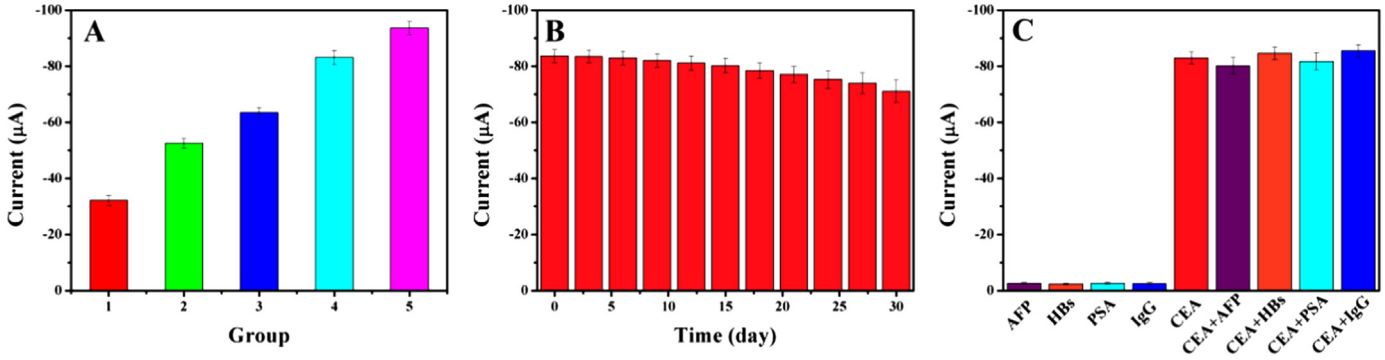


**Fig. 6.** (A) Current response of the immunosensor to detect 1 pg/mL, 10 pg/mL, 100 pg/mL, 1 ng/mL, 10 ng/mL of CEA; (B) current response of the immunosensor in different time; (C) current response of interfering substances (10 ng/mL) alone and compound of interfering substances and CEA (1 ng/mL). Error bar = SD (n = 5).

immunosensor with simple preparation, quick response and sensitive detection can be easily extended to the application for accurate clinical diseases diagnosis.

## Acknowledgments

This study was financially supported by the Key Research and Development Program of Shandong Province (No. 2018GSF120001), the National Natural Science Foundation of China (No. 21575079), the Project of Shandong Province Higher Educational Science and Technology Program (No. J14LC09). All of the authors express their deep thanks.

## Appendix A. Supporting information

Supplementary data associated with this article can be found in the online version at doi:10.1016/j.bios.2018.11.039.

## References

Alsabti, E., 1979. Carcinoembryonic antigen (CEA) as prognostic marker in colonic cancer. J. Surg. Oncol. 12 (2), 127–129.
Amani, J., Maleki, M., Khoshroo, A., Sobhani-Nasab, A., Rahimi-Nasrabadi, M., 2018. An electrochemical immunosensor based on poly p-phenylenediamine and graphene nanocomposite for detection of neuron-specific enolase via electrochemically amplified detection. Anal. Biochem. 548, 53–59.
Chen, Q., Yu, C., Gao, R., Gao, L., Li, Q., Yuan, G., He, J., 2016. A novel electrochemical immunosensor based on the rGO-TEPA-PTC-$NH_2$ and AuPt modified C60 bimetallic nanoclusters for the detection of Vangl1, a potential biomarker for dysontogenesis. Biosens. Bioelectron. 79, 364–370.
Chou, S.-F., Hsu, W.-L., Hwang, J.-M., Chen, C.-Y., 2004. Development of an immunosensor for human ferritin, a nonspecific tumor marker, based on surface plasmon resonance. Biosens. Bioelectron. 19 (9), 999–1005.
Felix, F.S., Angnes, L., 2017. Electrochemical immunosensors - a powerful tool for analytical applications. Biosens. Bioelectron. 102, 470–478.
Frens, G., 1973. Controlled nucleation for the regulation of the particle size in monodisperse gold suspensions. Nat. Phys. Sci. 241 (105), 20.
Gu, X., She, Z., Ma, T., Tian, S., Kraatz, H.-B., 2018. Electrochemical detection of carcinoembryonic antigen. Biosens. Bioelectron. 102, 610–616.
Guo, Y., Deng, L., Li, J., Guo, S., Wang, E., Dong, S., 2011. Hemin-graphene hybrid nanosheets with intrinsic peroxidase-like activity for label-free colorimetric detection of single-nucleotide polymorphism. ACS Nano 5 (2), 1282–1290.
Hummers Jr, W.S., Offeman, R.E., 1958. Preparation of graphitic oxide. J. Am. Chem. Soc. 80 (6) (1339-1339).
Li, J., Yuan, T., Yang, T., Xu, L., Zhang, L., Huang, L., Cheng, W., Ding, S., 2018a. DNA-grafted hemin with preferable catalytic properties than G-quadruplex/hemin for fluorescent miRNA biosensing. Sens. Actuators B: Chem. 271, 239–246.
Li, J., Jiang, J., Xu, Z., Liu, M., Tang, S., Yang, C., Qian, D., 2018b. Facile synthesis of Ag@$Cu_2O$ heterogeneous nanocrystals decorated N-doped reduced graphene oxide with enhanced electrocatalytic activity for ultrasensitive detection of $H_2O_2$. Sens. Actuators B: Chem. 260, 529–540.
Li, M., Wang, P., Li, F., Chu, Q., Li, Y., Dong, Y., 2017a. An ultrasensitive sandwich-type electrochemical immunosensor based on the signal amplification strategy of mesoporous core-shell Pd@Pt nanoparticles/amino group functionalized graphene nanocomposite. Biosens. Bioelectron. 87, 752–759.
Li, M., Wang, P., Pei, F., Yu, H., Dong, Y., Li, Y., Liu, Q., Chen, P., 2018c. A novel signal amplification system fabricated immunosensor based on Au nanoparticles and mesoporous trimetallic PdPtCu nanospheres for sensitive detection of prostate specific antigen. Sens. Actuators B: Chem. 261, 22–30.
Li, N.-L., Jia, L.-P., Ma, R.-N., Jia, W.-L., Lu, Y.-Y., Shi, S.-S., Wang, H.-S., 2017b. A novel sandwiched electrochemiluminescence immunosensor for the detection of carcinoembryonic antigen based on carbon quantum dots and signal amplification. Biosens. Bioelectron. 89, 453–460.
Li, Q., Tang, D., Lou, F., Yang, X., Chen, G., 2014. Simultaneous electrochemical multiplexed immunoassay of biomarkers based on multifunctionalized graphene nanotags. ChemElectroChem 1 (2), 441–447.
Liang, Z.-X., Song, H.-Y., Liao, S.-J., 2011. Hemin: a highly effective electrocatalyst mediating the oxygen reduction reaction. J. Phys. Chem. C. 115 (5), 2604–2610.
Ma, H., Li, X., Yan, T., Li, Y., Zhang, Y., Wu, D., Wei, Q., Du, B., 2016. Electrochemiluminescent immunosensing of prostate-specific antigen based on silver nanoparticles-doped Pb (II) metal-organic framework. Biosens. Bioelectron. 79, 379–385.
Majuri, M.L., Hakkarainen, M., Paavonen, T., Renkonen, R., 1994. Carcinoembryonic antigen is expressed on endothelial cells: a putative mediator of tumor cell extravasation and metastasis. Apmis 102 (1–6), 432–438.
Mani, V., Chikkaveeraiah, B.V., Patel, V., Gutkind, J.S., Rusling, J.F., 2009. Ultrasensitive immunosensor for cancer biomarker proteins using gold nanoparticle film electrodes and multienzyme-particle amplification. ACS Nano 3 (3), 585–594.
Rizwan, M., Elma, S., Lim, S.A., Ahmed, M.U., 2018. AuNPs/CNOs/SWCNTs/chitosan-nanocomposite modified electrochemical sensor for the label-free detection of carcinoembryonic antigen. Biosens. Bioelectron. 107, 211–217.
Singh, S., Tuteja, S.K., Sillu, D., Deep, A., Suri, C.R., 2016. Gold nanoparticles-reduced graphene oxide based electrochemical immunosensor for the cardiac biomarker myoglobin. Microchim. Acta 183 (5), 1729–1738.
Wischhusen, J., Padilla, F., 2017. Microbubble enzyme-linked immunosorbent assay for the detection of targeted microbubbles in vitro static binding assays. Ultrasound Med. Biol. 43 (7), 1506–1519.
Wu, D., Ma, H., Zhang, Y., Jia, H., Yan, T., Wei, Q., 2015. Corallite-like magnetic $Fe_3O_4$@$MnO_2$@ Pt nanocomposites as multiple signal amplifiers for the detection of carcinoembryonic antigen. ACS Appl. Mater. Interfaces 7 (33), 18786–18793.
Xue, T., Jiang, S., Qu, Y., Su, Q., Cheng, R., Dubin, S., Chiu, C.Y., Kaner, R., Huang, Y., Duan, X., 2012. Graphene-supported hemin as a highly active biomimetic oxidation catalyst. Angew. Chem. 124 (16), 3888–3891.
Zapp, E., Westphal, E., Gallardo, H., de Souza, B., Vieira, I.C., 2014. Liquid crystal and gold nanoparticles applied to electrochemical immunosensor for cardiac biomarker. Biosens. Bioelectron. 59, 127–133.
Zhang, H., Ma, L., Li, P., Zheng, J., 2016. A novel electrochemical immunosensor based on nonenzymatic Ag@Au-$Fe_3O_4$ nanoelectrocatalyst for protein biomarker detection. Biosens. Bioelectron. 85, 343–350.
Zhang, X., Li, Y., Lv, H., Feng, J., Gao, Z., Wang, P., Dong, Y., Liu, Q., Zhao, Z., 2018. Sandwich-type electrochemical immunosensor based on Au@Ag supported on functionalized phenolic resin microporous carbon spheres for ultrasensitive analysis of α-fetoprotein. Biosens. Bioelectron. 106, 142–148.